Chiral relaxation time at the crossover of quantum chromodynamics

M. Ruggieri,[1,*] G. X. Peng,[1,2,†] and M. Chernodub[3,4,‡]

[1]*College of Physics, University of Chinese Academy of Sciences, Yuquanlu 19A, Beijing 100049, China*
[2]*Theoretical Physics Center for Science Facilities, Institute of High Energy Physics, Beijing 100049, China*
[3]*CNRS, Laboratoire de Mathématiques et Physique Théorique UMR 7350, Université de Tours, Tours 37200, France*
[4]*Soft Matter Physics Laboratory, Far Eastern Federal University, Sukhanova 8, Vladivostok 690950, Russia*

(Received 4 July 2016; published 12 September 2016)

We study microscopic processes responsible for chirality flips in the thermal bath of quantum chromodynamics at finite temperature and zero baryon chemical potential. We focus on the temperature range where the crossover from chirally broken phase to quark-gluon plasma takes place, namely, $T \simeq (150, 200)$ MeV. The processes we consider are quark-quark scatterings mediated by collective excitations with the quantum number of pions and σ meson; hence we refer to these processes simply as one-pion (one-σ) exchanges. We use a Nambu-Jona-Lasinio model to compute equilibrium properties of the thermal bath, as well as the relevant scattering kernel to be used in the collision integral to estimate the chiral relaxation time τ. We find $\tau \simeq 0.1 \div 1$ fm/c around the chiral crossover.

DOI: 10.1103/PhysRevD.94.054011

I. INTRODUCTION

Interactions of fermions with nontrivial gauge field configurations carrying a finite winding number, Q_W, lead to chiral imbalance between the densities of right-handed, n_R, and left-handed, n_L, chiral fermions. The imbalance—induced via the Adler-Bell-Jackiw (ABJ) anomaly [1,2]—is characterized by the finite chiral density, $n_5 \equiv n_R - n_L$. In finite-temperature quantum chromodynamics (QCD) the topological gauge field configurations in Minkowski space are named sphalerons, whose production rate has been estimated to be quite large [3,4]. The large number of sphaleron transitions at high temperature suggests the possibility that net chirality might be abundant (locally) in the quark-gluon plasma phase of QCD. This observation stimulated many studies of various exotic effects; see [5–22] and references therein.

In order to describe equilibrium systems with a finite chiral density $n_5 \neq 0$ it is customary to introduce the chiral chemical potential, μ_5, conjugated to the chiral density n_5 [23–42]. Because of the chiral ABJ anomaly as well as chirality-changing processes the chiral density n_5 is not a strictly conserved quantity. One might, however, assume that the chiral chemical potential $\mu_5 \neq 0$ describes a system in thermodynamical equilibrium with a fixed value of the chiral charge n_5 on a time scale much larger than the typical chiral relaxation time scale τ that is needed for n_5 to equilibrate. For example, this equilibration has been recently studied in [23] where n_5 is generated dynamically via the chiral anomaly activated by the simultaneous presence of parallel electric and magnetic fields.

In this article we compute the chiral relaxation time, τ, in a two flavor Nambu-Jona-Lasinio (NJL) model that is invoked to mimic the QCD thermal bath in the temperature range $T \simeq (150, 200)$ MeV where the crossover from color confinement phase to quark-gluon plasma takes place. The main processes we consider are quark-quark scatterings mediated by collective excitations with the quantum numbers of pions; hence we simply call these processes one-pion exchange. We also consider, for completeness, scattering mediated by σ-meson exchange, which, however, is less relevant both because of the larger σ mass and because of the smaller weight of the diagrams with σ exchange compared to the ones with a pion exchange.

We use the NJL model to evaluate the chiral condensate at finite temperature, which allows us to compute the constituent quark mass in the thermal bath. Once the quark mass is known, we use the well-established NJL formalism to compute the scattering kernel of the microscopic processes we consider, and the collision integral (which represents the main numerical computation of this work) that allows us to estimate the relaxation time of chirality. The main result of our article is that we find $\tau \simeq 0.1 \div 1$ fm in the aforementioned crossover temperature range. We also find that the relaxation time decreases with temperature, regardless of the fact that chiral symmetry gets partially restored at the crossover. This is explained by taking into account that although the scattering kernel of chirality flipping processes becomes smaller with increasing temperature, the portion of phase space for the scattering increases with temperature, eventually leading to an increase of the scattering rate and a lowering of the

*marco.ruggieri@ucas.ac.cn
†gxpeng@ucas.ac.cn
‡maxim.chernodub@lmpt.univ-tours.fr

relaxation time. The behavior of τ versus temperature computed here is in some disagreement with the ansatz $\tau \propto 1/M_q$ used in Ref. [23], where M_q corresponds to the constituent quark mass, which was admittedly too simple as it did not take into account properly the phase space opening at finite temperature.

We also consider a computation in which we merge by hand the NJL model below the critical temperature with a quasiparticle model above the critical temperature: the latter differs from NJL because the quasiparticle thermal mass, which is obtained by a numerical fit of Lattice data about pressure, entropy, and energy density, is assumed to arise as a pole in the propagator dressed with a chiral invariant self-energy rather than from a term $\propto \bar{\psi}\psi$ in the Lagrangian. This thermal mass is generated by many body effects that are not present in a mean field NJL: in fact the latter describes only the constituent mass arising from both spontaneous and explicit chiral symmetry breaking. In quasiparticle models the thermal mass is generally found to be large around the chiral crossover and increasing with temperature [43–52]; this large mass suppresses thermal quark excitations; therefore, we expect that interpolating between NJL and quasiparticles around the chiral crossover will lower the collision rate, and hence increase the relaxation time. This rough idea is in agreement with our results. We do not, however, push very much the results of this calculation since it is far from being rigorous: our only purpose is to illustrate how the collision rate would be affected if beside the NJL constituent quark mass one introduces in an effective way many body effects encoded in a large thermal mass above T_c.

The plan of the article is as follows. In Sec. II we state the problem and set up the main equations needed to compute the relaxation time. In Sec. III we discuss the one-meson exchange within the NJL model. In Sec. IV we summarize our main findings, in particular, the relaxation time shown in Figs. 4 and 8. Finally, in Sec. V we draw our conclusions.

II. RELAXATION TIME OF CHIRAL DENSITY

The main aim of this article is to compute the relaxation time τ for chirality flips $R \leftrightarrow L$ in a thermal bath at given temperature T. In our effective-model approach the specific microscopic process responsible for the chirality flips is the pion exchange between left- and right-handed quarks. We discuss this process in detail below. In this section we begin with a brief statement of the problem of chiral density relaxation, then we define the microscopic process that changes chirality in the thermal bath and compute the relevant scattering matrix.

In order to state the problem we consider quark matter in the background of parallel electric and magnetic fields [23,53–55]. In this case the evolution of the chiral density n_5 with time is given by

$$\frac{dn_5}{dt} = -n_5\Gamma + N_c\frac{(eE)(eB)}{2\pi^2}\sum_f q_f^2 e^{-\frac{\pi M^2}{|q_f eE|}}, \qquad (1)$$

where the first term on the right-hand side describes a relaxation of the chiral density due to chirality-changing processes in the thermal medium, while the second term comes from the ABJ chiral anomaly supplemented with the exponential prefactor that takes into account the finiteness of the quark mass M. The quantity Γ in Eq. (1) corresponds to the rate of the chirality flips while its inverse defines the chiral relaxation time,

$$\tau = 1/\Gamma. \qquad (2)$$

Physically, Eq. (1) indicates that in parallel electric and magnetic external fields the ABJ anomaly creates a chiral imbalance n_5. According to the second term of Eq. (1), the chiral density should start to grow linearly with time if even the chiral imbalance was initially absent in the system, $n_5 = 0$. This process would continue forever—as long as the external fields are not screened by the media—if there were no other processes in the system. However, in the thermal bath certain microscopic processes may flip the chirality of quarks and the significance of the chirality-flipping process increases with the increase of the chiral density n_5. These processes are encoded in the first term in Eq. (1) where Γ is the chirality-changing rate that defines the characteristic chiral relaxation time τ, Eq. (2). If one waits long enough, $t \gg \tau$, the value of chiral density n_5 exponentially equilibrates at the following value:

$$n_5^{\rm eq} = N_c\frac{(eE)(eB)}{2\pi^2}\tau\sum_f q_f^2 e^{-\frac{\pi M^2}{|q_f eE|}}. \qquad (3)$$

The knowledge of the relaxation time τ is therefore crucial since it allows us to determine the equilibrium value of chiral density, $n_5^{\rm eq}$, and to compute the thermodynamically conjugated chiral chemical potential μ_5.

As we describe in more detail below, the microscopic processes we are interested in are quark-quark scattering mediated by collective modes with the quantum numbers of pions; hence we refer to these processes as one-pion exchange for simplicity. The computation of τ for the physical setup described above—i.e., for the system of quarks in external electromagnetic fields—is too complicated because the external fields create a finite chiral density n_5 that is associated with nonzero chiral chemical potential μ_5; the nonzero μ_5 and the fields affect the quark propagators, indirectly changing meson properties and scattering amplitudes, making the consistent calculation very tough. Therefore, here we limit ourselves to a much simpler problem, namely, the computation of relaxation time τ for a system without external fields at a negligibly small value of the chiral chemical potential $\mu_5 \ll T$. In this

paper we are not interested in a concrete physical mechanism that creates the chiral imbalance. A similar approach has already been used in [56] to estimate τ in quark-gluon plasma, where gluon- and photon-mediated Compton scattering processes have been taken as the microscopic mechanisms for chirality flips in the thermal bath. Here we differ from Ref. [56] because in the region of the chiral crossover the pion-exchange processes are much more effective compared to the Compton scattering.[1]

By the very definition of the chiral density,

$$n_5 = N_c N_f \int \frac{d^3p}{(2\pi)^3}(f_R - f_L), \tag{4}$$

where $f_{R,L}$ denote distribution functions for the right-handed and left-handed quarks, respectively, we get

$$\frac{dn_5}{dt} = N_c N_f \int \frac{d^3p}{(2\pi)^3}\left(\frac{df_R}{dt} - \frac{df_L}{dt}\right). \tag{5}$$

The overall $N_c N_f$ takes into account that n_5 is defined as a sum over color and flavor; keeping this in mind, $f_{R,L}$ denote distribution functions for a quark with color and flavor fixed. Time evolution of $f_{R,L}$ is given by the Boltzmann collision integral,

$$\frac{df_R(p)}{dt} = \int d\Pi \frac{(2\pi)^4\delta^4(p+k-p'-k')}{2E_p}|\mathcal{M}|^2 F, \tag{6}$$

where $d\Pi$ corresponds to the standard momentum space measure,

$$d\Pi = \frac{d^3k}{(2\pi)^3 2E_k}\frac{d^3k'}{(2\pi)^3 2E'_k}\frac{d^3p'}{(2\pi)^3 2E'_p}, \tag{7}$$

and the kernel F takes into account the population of the incoming and outgoing particles in the process. In Eq. (6) the squared transition amplitude $|\mathcal{M}|^2$ is the main ingredient in the collision integral and it can be computed once a microscopic process has been chosen.

The microscopic processes on which we focus in this article are the transitions $q_R q_R \to q_L q_L$ and vice versa. The change of chiral density produced by these processes would cancel if the thermal bath is chirally balanced, $\mu_5 = 0$. However, the presence of the chiral imbalance $\mu_5 \neq 0$ implies a different population of R- and L-handed quarks, which in turn results in a finite rate for the chiral density equilibration. Given this microscopic process it is possible to specify the kernel $F(p,k,p',k')$ in Eq. (6). In this study we consider the simple case of the classical Boltzmann kernel, namely,

$$F(p,k,p',k') = f_L(p')f_L(k') - f_R(p)f_R(k) \tag{8}$$

for the scattering of two incoming R quarks giving two outgoing L quarks. The Boltzmann distribution functions are defined as

$$f_{R/L}(p) = e^{-\beta\omega_\pm}, \tag{9}$$

where the dispersion relation is

$$\omega_s = \sqrt{(p + s\mu_5)^2 + M_q^2}, \qquad s = \pm 1. \tag{10}$$

We also consider the Fermi-Dirac kernel,

$$\begin{aligned} F(p,k,p',k') = {} & f_L(p')f_L(k')[1 - f_R(p)][1 - f_R(k)] \\ & - f_R(p)f_R(k)[1 - f_L(p')][1 - f_L(k')], \end{aligned} \tag{11}$$

where the distribution functions

$$f_{R/L}(p) = \frac{1}{1 + e^{\beta\omega_\pm}} \tag{12}$$

correctly take into account the Pauli blocking due to the fermionic nature of quarks.

For simplicity we limit ourselves to consider the lowest order in μ_5/T in the collision integral (6). When we combine df_R/dt and df_L/dt in Eq. (5) we take into account that

$$\frac{df_L}{dt} = \frac{df_R}{dt}(\mu_5 \to -\mu_5), \tag{13}$$

so only the odd part in μ_5 contributes to dn_5/dt. It is easy to verify that both the Dirac delta argument and the four energies in the denominator are even functions of μ_5; thus, it is enough to consider these at $\mu_5 = 0$ and expand $F(p,k,p',k')$ in Eq. (8) up to the first order in μ_5/T. Writing

$$\frac{df_R}{dt} = \mathcal{A}(p) + \mu_5\mathcal{B}(p) + O(\mu_5^2) \tag{14}$$

and taking into account Eq. (13) we have

$$\frac{dn_5}{dt} = 2N_c N_f \mu_5 \int \frac{d^3p}{(2\pi)^3}\mathcal{B}(p), \tag{15}$$

where we have taken into account the color-flavor degeneracy; the squared matrix element to use in Eq. (15) is given by Eq. (48). The collision rate for chirality change, Γ, is obtained from Eq. (1), namely,

[1]Using explicit expressions of Ref. [56] we estimated that the pion-mediated processes—with the relaxation time given in our Fig. 8 below—are about 1 or even 2 orders of magnitude faster compared to the Compton scattering.

$$\Gamma = -\frac{1}{n_5}\frac{dn_5}{dt}, \tag{16}$$

and the relaxation time is then computed by Eq. (2).

In order to relate the chiral density to the chiral chemical potential we use the NJL model at finite μ_5 [26,27], limiting ourselves to the leading order in μ_5/T. The chiral density n_5 can be computed as $n_5 = -\partial\Omega/\partial\mu_5$ where Ω is the thermodynamic potential,

$$\Omega = \Omega_{MF} + \Omega_v + \Omega_T, \tag{17}$$

with

$$\Omega_{MF} = \frac{(M_q - m_0)^2}{4G}, \tag{18}$$

$$\Omega_v = -N_c N_f \sum_{s=\pm 1} \int \frac{d^3p}{(2\pi)^3}\omega_s, \tag{19}$$

$$\Omega_T = -2N_c N_f T \sum_{s=\pm 1} \int \frac{d^3p}{(2\pi)^3}\log\left(1 + e^{-\beta\omega_s}\right). \tag{20}$$

In the above equations $M_q = m_0 - 2G\langle\bar{q}q\rangle$ with $\langle\bar{q}q\rangle = \langle\bar{u}u\rangle + \langle\bar{d}d\rangle$ corresponding to the chiral condensate. To obtain the chiral density as a function of μ_5 we expand Eq. (17) up to $O(\mu_5^2 T^2)$,

$$\Omega = \Omega_0 + \mu_5^2(L_0 + L_T), \tag{21}$$

where Ω_0 corresponds to the thermodynamic potential for $\mu_5 = 0$, namely,

$$\Omega_0 = \frac{(M_q - m_0)^2}{4G} - 2N_c N_f \int \frac{d^3p}{(2\pi)^3}\omega - 4N_c N_f T \times \int \frac{d^3p}{(2\pi)^3}\log\left(1 + e^{-\beta\omega}\right), \tag{22}$$

with $\omega = \sqrt{p^2 + M_q^2}$.

The term quadratic in μ_5 in Eq. (21) comes with the prefactors,

$$L_0 = -\frac{N_c N_f}{2\pi^2} M_q^2 \int_0^\Lambda dp \frac{p^2}{(p^2 + M_q^2)^{3/2}}, \tag{23}$$

$$L_T = -\frac{N_c N_f}{\pi^2} \int_0^\infty dp \frac{p^2}{(p^2 + M_q^2)^{3/2}} \times \frac{(-M_q^2 e^{\beta\omega} + \beta p^2 \omega e^{\beta\omega} - M_q^2)}{(e^{\beta\omega} + 1)^2}. \tag{24}$$

By virtue of the equations above we can write

$$n_5 = -2\mu_5(L_0 + L_T). \tag{25}$$

It can be easily verified that L_0 vanishes for $M_q = 0$. On the other hand in the limit of vanishing quark mass the above equation leads to $n_5 = N_c N_f \mu_5 T^2/3$ in agreement with Ref. [6].

Divergent ultraviolet integrals in the above equations are regulated by a hard cutoff Λ, where Λ is considered as one of the parameters of the model and its value is fixed by phenomenological requirements together with the NJL coupling, G, and the bare quark mass. The parameter set we use is $\Lambda = 653$ MeV, $m_0 = 5.39$ MeV, and $G = 2.14/\Lambda^2$. Taking into account Eqs. (15), (16), and (25) we can write the rate for the chirality change as

$$\Gamma = \frac{N_c N_f}{L_0 + L_T} \int \frac{d^3p}{(2\pi)^3}\mathcal{B}(p), \tag{26}$$

with $\mathcal{B}(p)$ defined in Eq. (14). The relaxation time for chirality is then given by Eq. (2).

III. ONE-MESON EXCHANGE WITHIN THE NJL MODEL

We are interested in interaction channels that lead to a change of chiral density in the thermal bath. Here we focus on one-pion exchange, which should be the dominant process around the chiral crossover. We also consider scattering mediated by the σ meson but its contribution to the collision rate is found to be smaller than the one obtained by one-pion exchange. We assume that quarks are in equilibrium in a thermal bath with temperature T and chiral chemical potential $\mu_5 \neq 0$ (a vanishing μ_5 would lead to a zero net chiral density change by this process) and we focus on transitions $q_R q_R \to q_L q_L$ and $q_L q_L \to q_R q_R$. Strictly speaking, a system with the chiral imbalance, $\mu_5 \neq 0$, cannot be in thermal equilibrium due to chirality-changing processes that are the subject of this article. However, we assume that there is a process that pumps the chiral charge into the system so that the mean chiral density and, consequently, the chiral chemical potential, are both nonzero. The chiral charge may be pumped into the system by the chiral anomaly in the background of parallel electric and magnetic fields (see, e.g., Ref. [23] for the relevant discussion in the context of the NJL model).

A. Quark-pion scattering kernel

In order to compute the rate for chirality-changing processes (2) in the medium close to the chiral phase transition we use a two flavor NJL model [57,58] (see [59,60] for reviews) with Lagrangian density given by

$$\mathcal{L} = \bar{q}(i\gamma_\mu\partial^\mu - m_0)q + \mathcal{L}_4, \tag{27}$$

where q denotes a quark field with Dirac, color, and flavor indices and m_0 is the current quark mass. In the above equation the interaction Lagrangian, $\mathcal{L}_4$, is given by

$$\mathcal{L}_4 = G[(\bar{q}q)^2 + (\bar{q}i\gamma_5\boldsymbol{\tau}q)^2], \tag{28}$$

which is invariant under the $SU(2)_V \otimes SU(2)_A \otimes U(1)_V$ group, and G is a coupling constant with mass dimension $d = -2$. Introducing the collective fields $\sigma = G\bar{q}q$, $\boldsymbol{\pi} = G\bar{q}i\gamma_5\boldsymbol{\tau}q$, after a Hubbard-Stratonovich transformation the interaction term $\mathcal{L}_4$ can be written as

$$\mathcal{L}_4 = 2G\langle\bar{q}q\rangle\bar{q}q + \bar{q}[g^0_{\sigma qq}\sigma + g^0_{\pi qq}i\gamma_5\boldsymbol{\tau}\cdot\boldsymbol{\pi}]q - \frac{(G\langle\bar{q}q\rangle + \sigma)^2 + \boldsymbol{\pi}^2}{G}, \tag{29}$$

where we have introduced the bare quark-meson couplings $g^0_{\sigma qq} = g^0_{\pi qq} = 2$. The bare couplings get renormalized by quark interactions in the medium and they give effective quark-meson couplings. From now on we denote by σ the quantum fluctuation of the collective field $G\bar{q}q$ on the top of its expectation value $G\langle\bar{q}q\rangle$. In the partition function of the model specified by Lagrangian (29) an integration over quark and meson fields is understood; the Lagrangian is quadratic in quark fields so the functional integral can be done exactly and one is left with an effective Lagrangian for meson fields, whose in-medium propagators can be computed easily by the random phase approximation; it is then possible to write an effective quark-quark interaction due to one-meson exchange. Since this topic is well established in the literature, below we quote, without derivations, the basic equations relevant for the present study and refer the interested reader to the review [59] for further details. We first focus on the one-pion exchange as it is the dominant process in the temperature range of our interest; the description of σ-meson exchange can be obtained easily once the formalism for the pion exchange is established.

From Eq. (29) we can extract the quark-pion interaction at the tree level,

$$\mathcal{L}_{\pi qq} = ig^0_{\pi qq}\bar{q}\gamma_5\boldsymbol{\tau}\cdot\boldsymbol{\pi}q = ig^0_{\pi qq}(\bar{q}_L\boldsymbol{\tau}\cdot\boldsymbol{\pi}q_R - \bar{q}_R\boldsymbol{\tau}\cdot\boldsymbol{\pi}q_L), \tag{30}$$

where we have made explicit the change of chirality of quarks due to the interaction with a pionlike collective excitation. Therefore, it is possible to change the net chirality of the system by virtue of processes $q_Rq_R \to q_Lq_L$ and vice versa. The change of chiral density produced by these processes would cancel if in the thermal bath $\mu_5 = 0$; however, assuming $\mu_5 \neq 0$ implies a different population of R- and L-handed quarks, which in turn results in a finite rate for chiral density equilibration given in (26) and (2).

The amplitude for the scattering process $qq \to qq$ due to one-pion exchange can be written as

$$i\mathcal{M} = i\bar{q}_{ai}q_{bj}\bar{q}_{ck}q_{d\ell}(U_{\alpha\beta})^{abcd}_{ijk\ell}, \tag{31}$$

where $a, \ldots, d$ denote Dirac indices and $i, \ldots, \ell$ correspond to flavor indices (one-meson exchange is blind to color hence there is no need to introduce a color index in the above equation). The scattering kernel, U, is given in the random phase approximation by

$$i(U_{\alpha\beta})^{abcd}_{ijk\ell} = i(\mathcal{T}_\alpha)^{ab}_{ij}\frac{2G}{1-2G\Pi}(\mathcal{T}_\beta)^{cd}_{k\ell}, \tag{32}$$

where interaction vertex $\mathcal{T}$ carries Dirac and flavor structure and depends on the particular interaction channel,

$$\mathcal{T}_\alpha = i\gamma_5 \otimes T_\alpha. \tag{33}$$

For π_0 exchange $\mathcal{T}_\alpha = \mathcal{T}_\beta = \sigma_3$ with σ_3 being the third Pauli matrix in flavor space; for $\pi^\pm$ exchange one has to use the combinations

$$\tau^\pm = \frac{1}{\sqrt{2}}(\sigma_1 \pm \sigma_2). \tag{34}$$

However, the scattering amplitude does not depend on the particular channel chosen among the neutral and charged pion exchanges (neglecting the small mass difference between $\pi^\pm$ and π_0); therefore, from now on we suppress the greek indices and focus on π_0 exchange. From Eq. (32) it is possible to read the in-medium meson propagator in momentum space,

$$D(k^2) = \frac{2G}{1-2G\Pi(k^2)}, \tag{35}$$

where the pion self-energy is given by

$$\Pi(k^2) = -i\mathrm{Tr}\int\frac{d^4p}{(2\pi)^4}\gamma_5\sigma_3S(p)\gamma_5\sigma_3S(p-k). \tag{36}$$

A standard algebraic manipulation leads to [59]

$$\Pi(k_0,\boldsymbol{k}) = \frac{1}{2G}\left(1 - \frac{m_0}{M_q}\right) + 2N_cN_fk^2I(k^2), \tag{37}$$

where[2]

$$I(k_0,\boldsymbol{k}) = -i\int\frac{d^4p}{(2\pi)^4}\frac{1}{(p^2-M_q^2)[(p-k)^2-M_q^2]} \tag{38}$$

[2]Our definition of I differs from the one of [59] for an overall $-i$.

and $k^\mu = (k_0, \boldsymbol{k})$ on the right-hand side of the above equation.

B. σ-quark scattering kernel

The formalism set up in the previous section for the quark-pion scattering can be adapted easily to the description of the scattering kernel of quarks with the σ meson. In particular, the amplitude for the scattering process $qq \to qq$ due to one-σ exchange can be written analogously to Eq. (31), namely,

$$i\mathcal{M} = i\bar{q}_{ai}q_{bj}\bar{q}_{ck}q_{d\ell}(U)^{abcd}_{ijk\ell}, \tag{39}$$

with the scattering kernel within the random phase approximation given by

$$i(U)^{abcd}_{ijk\ell} = i(\mathcal{T})^{ab}_{ij}\frac{2G}{1-2G\Pi_\sigma}(\mathcal{T})^{cd}_{k\ell}, \tag{40}$$

and

$$\mathcal{T} = \boldsymbol{1}_D \otimes \boldsymbol{1}_F, \tag{41}$$

where 1_D and 1_F denote the identity in Dirac and flavor spaces, respectively. From Eq. (40) it is possible to read the in-medium σ propagator in momentum space,

$$D_\sigma(k^2) = \frac{2G}{1-2G\Pi_\sigma(k^2)}, \tag{42}$$

with self-energy given by

$$\Pi_\sigma(k^2) = -i\mathrm{Tr}\int\frac{d^4p}{(2\pi)^4}\gamma_5\sigma_3 S(p)\gamma_5\sigma_3 S(p-k). \tag{43}$$

A standard algebraic manipulation leads to [59]

$$\Pi_\sigma(k_0,\boldsymbol{k}) = \frac{1}{2G}\left(1-\frac{m_0}{M_q}\right) + 2N_cN_f(k^2-4M_q^2)I(k^2), \tag{44}$$

with I defined in Eq. (38).

C. Scattering amplitude: π exchange

By means of the one-pion exchange it is possible to write several diagrams giving contribution to the scattering amplitude, represented in Fig. 1 for the case of an incoming u_R quark. We assume equal mass for charged and neutral pions, and $\mu_{5u} = \mu_{5d}$: in this way the one-pion exchange is blind to quark flavor and the scattering amplitude is independent of the particular current chosen. Given a quark with color and flavor fixed, for the π_0 exchange there are two possible processes, namely, (a) and (b) in Fig. 1, and the charged pion exchange adds one further process denoted by (c) in Fig. 1. In this isospin symmetric limit the three diagrams in Fig. 1 give the same result. We denote by $\mathcal{M}_i$ the antisimmetrized amplitude corresponding to diagram (i) with $i = a, b, c$. For each of the diagrams with an incoming u_R quark in Fig. 1 we sum incoherently on the color of the second incoming quark (namely, cross sections are summed rather than amplitudes): this brings an overall N_c to the total cross section. In addition we sum incoherently over flavors, considering however that diagrams (b) and (c) correspond to the same initial and final states so the corresponding amplitudes should add coherently. Therefore, we can write the squared amplitude as

$$|\mathcal{M}|^2 = N_c|\mathcal{M}_a|^2 + N_c|\mathcal{M}_b + \mathcal{M}_c|^2. \tag{45}$$

Since in the isospin symmetric limit the amplitude $\mathcal{M}_i$ does not depend on the index i we can write

$$|\mathcal{M}|^2 = N_c(1+4)|\mathcal{M}_a|^2. \tag{46}$$

The calculation of the transition amplitude is quite standard: the only detail to take into account is the projection of initial and final states onto chirality eigenstates. This is achieved noticing that the current can be written as $\bar{q}_L\gamma_5 q_R = \bar{q}\gamma_5 P_R q$, where $P_R = (1+\gamma_5)/2$ and a similar relation holds for the current changing an incoming left to an outgoing right. Therefore, we can use all the standard technology for tree level calculations of transition amplitudes forgetting the selection of chirality in the spinors, because it is automatically implemented thanks to the chirality projector. In the isospin symmetric limit we

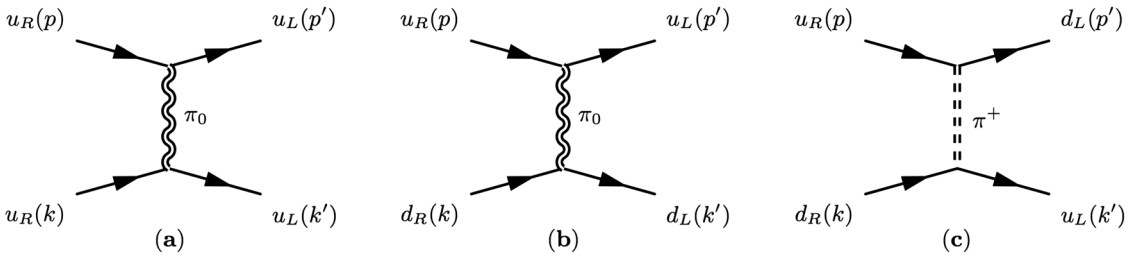

FIG. 1. Diagrams (a) and (b) correspond to neutral pion exchange; diagram (c) corresponds to charged pion exchange. Tree level diagrams for the chirality flips of u quarks due to one-pion exchange.

find that the diagrams in Fig. 1 give the same contribution. We obtain

$$\mathcal{M}_a = D(t)(\bar{u}'_{p'}\gamma_5 P_R u_p)(\bar{u}'_{k'}\gamma_5 P_R u_k) - D(u)(\bar{u}'_{k'}\gamma_5 P_R u_1)(\bar{u}'_{p'}\gamma_5 P_R u_2); \quad (47)$$

here the prime denotes outgoing particles, labels 1 and 2 label the particle, and u and t denote standard Mandelstam variables. In writing Eq. (47) we have ignored all the overall i since they do not affect the squared matrix element. Taking into account that for each color of the incoming quark p there are N_c possible colors of the incoming k for the scattering, and that the scattering involving different colors sums up incoherently, we can write the squared matrix element as

$$|\mathcal{M}|^2_{\pi qq} = \frac{1}{4}[4N_c(1+4)D(t)D^\dagger(t)a_1 + 4N_c(1+4)D(u)D^\dagger(u)a_2 - 2N_c(1+4)D_{tu}(a_1+a_2-a_3)], \quad (48)$$

with $D_{tu} = D(t)D^\dagger(u) + D(u)D^\dagger(t)$ and a_i defined as

$$a_1 = \frac{(t-2M_q)^2}{4}, \quad (49)$$

$$a_2 = \frac{(u-2M_q)^2}{4}, \quad (50)$$

$$a_3 = \frac{(s-2M_q)^2}{4}, \quad (51)$$

with t, u, and s denoting the Mandelstam variables. The overall factor $1/4$ in Eq. (48) takes into account the average over initial spins and sum over final spins.

From Eq. (48) we notice that the scattering takes place in the t and u channels: because $t \le 0$ and $u \le 0$ the in-medium pion propagator is probed by spacelike virtual momenta and the pion self-energy $\Pi(k_0, \boldsymbol{k})$, which is the main ingredient in the scattering kernel in Eq. (32), has to be computed for $k^2 \le 0$. After analytic continuation to imaginary time and using the Matsubara formalism to deal with loop integrals at finite temperature we find

$$I(k_0,\boldsymbol{k}) = -\int \frac{d^3p}{(2\pi)^3}\left[\frac{A}{k_0+E_p+E_{pk}} + \frac{B}{k_0-E_p-E_{pk}}\right], \quad (52)$$

where we have defined

$$E_p = \sqrt{p^2+M_q^2}, \quad E_{pk} = \sqrt{(\boldsymbol{p}-\boldsymbol{k})^2+M_q^2}, \quad (53)$$

and

$$A = \frac{1}{4E_p}\frac{\tanh(E_p/(2\beta))}{k_0+E_p-E_{pk}} + \frac{1}{4E_{pk}}\frac{\tanh(E_{pk}/(2\beta))}{k_0-E_p+E_{pk}}, \quad (54)$$

$$B = \frac{1}{4E_p}\frac{\tanh(E_p/(2\beta))}{k_0-E_p+E_{pk}} + \frac{1}{4E_{pk}}\frac{\tanh(E_{pk}/(2\beta))}{k_0+E_p-E_{pk}}. \quad (55)$$

In Eq. (52) we have made explicit the poles at $k_0 = \pm(E_p+E_{pk})$ that, once treated by the $i\varepsilon$ prescription to build a Feynman propagator, are responsible for the pion instability towards creation of quark-antiquark pairs; in a similar way in Eq. (54) we have split the contributions in terms of functions that become singular when $k_0 = \pm(E_p-E_{kp})$ that still give an imaginary part and are related to pion emission and absorption processes by quarks.

In the processes of interest in the present article only the latter poles are relevant: as a matter of fact being $k^2 \le 0$ implies $k_0^2 \le \boldsymbol{k}^2$; it is easy to realize that this condition forces $E_p + E_{pk} > |k_0|$ for any value of k_0, hence removing the singularities $\propto [k_0 \pm (E_p+E_{pk})]^{-1}$ from the $\boldsymbol{p}$ space. Physically this means that the only contribution of the imaginary part of the scattering kernel is related to emission and absorption processes. Taking into account only the emission-absorption poles the real and imaginary parts of I in Eq. (52) can be easily obtained: treating the poles by the standard $i\varepsilon$ prescription to build a Feynman propagator and using the Sokhotski-Plemelj theorem,

$$\frac{1}{x-x_0\pm i\varepsilon} = \mp\, i\pi\delta(x-x_0) + \mathrm{PV}\frac{1}{x-x_0}, \quad (56)$$

where PV corresponds to the principal value, we find

$$\Im I(k_0,\boldsymbol{k}) = \mathrm{sign}(k_0)\pi\int\frac{d^3p}{(2\pi)^3}\left[\frac{1}{4E_p}\frac{\tanh(E_p/(2\beta))}{k_0+E_p+E_{pk}} + \frac{1}{4E_{pk}}\frac{\tanh(E_{pk}/(2\beta))}{k_0-E_p-E_{pk}}\right]\delta(k_0+E_p-E_{pk}) + \mathrm{sign}(k_0)\pi\int\frac{d^3p}{(2\pi)^3}\left[\frac{1}{4E_p}\frac{\tanh(E_p/(2\beta))}{k_0-E_p-E_{pk}} + \frac{1}{4E_{pk}}\frac{\tanh(E_{pk}/(2\beta))}{k_0+E_p+E_{pk}}\right]\delta(k_0-E_p+E_{pk}). \quad (57)$$

We can resolve easily the two δ functions in Eq. (57),

$$\Im I(k_0,\boldsymbol{k}) = \mathrm{sign}(k_0)\pi \int \frac{d^3p}{(2\pi)^3}\frac{1}{|g'(P_\pm)|}\left[\frac{\tanh(E_p/(2\beta))}{4E_p}+\frac{\tanh(E_{pk}/(2\beta))}{4E_{pk}}\right] \times\left(\frac{1}{k_0-E_p-E_{pk}}+\frac{1}{k_0+E_p+E_{pk}}\right)(\delta(p_x-P_+)+\delta(p_x-P_-)), \quad (58)$$

where $P_\pm$ are the two solutions of the equation

$$g(p_x)\equiv k_0+E_p-E_{pk}=0, \quad (59)$$

satisfying $P_-=-P_+$, and g' denotes the derivative of g with respect to p_x, whose absolute value can be easily proved to be independent on the sign of p_x. The real part of I is then obtained by taking the principal value of Eq. (52).

D. Scattering amplitude: σ exchange

For the scattering amplitude of chirality change due to σ exchange we can follow the same lines of the previous section. In this case the relevant diagrams are depicted in Fig. 2, which we sum incoherently in color and flavor. In the isospin symmetric limit, however, the two diagrams coincide. Instead of Eq. (48) we have

$$|\mathcal{M}|^2_{\sigma qq} = \frac{1}{4}[4N_c(1+1)D_\sigma(t)D^\dagger_\sigma(t)a_1 + 4N_c(1+1)D_\sigma(u)D^\dagger_\sigma(u)a_2 - 2N_c(1+1)D_{tu}(a_1+a_2-a_3)], \quad (60)$$

with D_σ given by Eq. (42), $D_{tu}=D_\sigma(t)D^\dagger_\sigma(u)+D_\sigma(u)D^\dagger_\sigma(t)$, and a_i defined as in Eq. (48). For the real and imaginary part of Π_σ the arguments given above for the pion self-energy are still valid; hence we do not repeat them here.

Before going ahead we remark that a full calculation would amount to considering the interference between the diagrams for σ and pion exchange. We do not do this in our work for simplicity; this decision is partly justified *a posteriori* by the fact that we find that the collision rate due to σ exchange is always smaller than the one due to pion exchange; hence we expect that the interference of the two processes does not considerably affect our results.

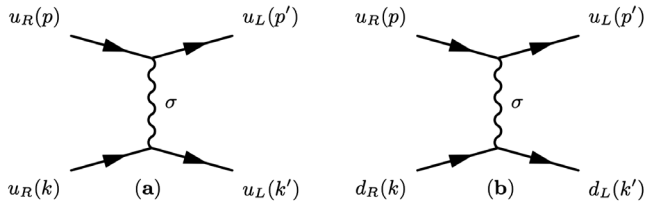

FIG. 2. Diagram (a) corresponds to $u-u$ quarks scattering, while diagram (b) denotes $u-d$ scattering. Tree level diagrams for the chirality flips of u quarks due to σ exchange.

IV. RESULTS

A. The NJL model

In Fig. 3 we show by the green dashed line M_q versus temperature, computed by minimization of the thermodynamic potential in the NJL model at $\mu_5=0$ given by Eq. (22). We need this quantity as it enters into the collision integral (15) via quark distribution functions and squared matrix element (48). It also enters into the relation between n_5 and μ_5 Eq. (25). From data shown in Fig. 3 we notice a rapid decrease of M_q in the temperature range (150,200) MeV, connecting a low-temperature phase where chiral symmetry is spontaneously broken to a high-temperature phase where chiral symmetry is approximately restored. In Fig. 3 we also plot our results for masses of pions and the σ meson, denoted respectively by m_π and m_σ, for later reference. By the inflection point of M_q we can define a pseudocritical temperature, $T_c\simeq 175$ MeV, for chiral symmetry restoration.

Next we turn to the computation of the relaxation time of chiral density. The main task is to compute the 12-dimensional integral in Eq. (26). We use the three-dimensional Dirac delta to perform the integral over d^3p' trivially; a change of variables (namely, a rigid rotation) allows us to take $\boldsymbol{p}$ along the z axis implying $\int d^3p = 4\pi\int p^2dp$. The Dirac delta expressing energy conservation is used to integrate over k_z. Eventually we are left with a six-dimensional integral over $p^2dpd^2k_Td^3k'$ with $d^2k_T=dk_xdk_y$. We perform this integral numerically

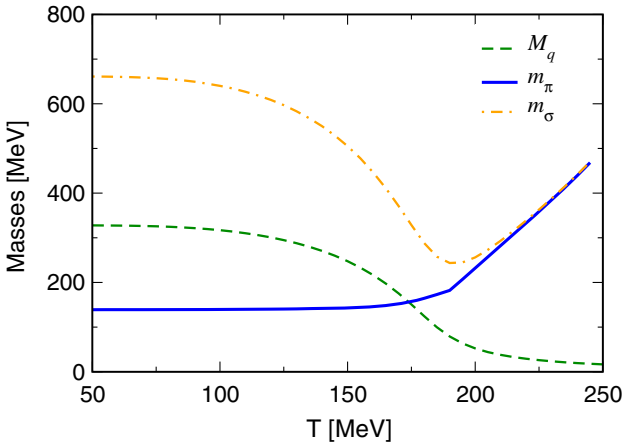

FIG. 3. M_q (green dashed line), m_π (solid blue line), and m_σ (orange dot-dashed line) versus temperature.

by a quasi-Monte Carlo routine [61,62] that uses the MISER Monte Carlo adaptive algorithm [63,64] with a Sobol low discrepancy sequence [65] in place of a uniform random sequence. The integration variables are scaled in units of temperature T, and we cut off integrals at $10T$.

In Fig. 4 we plot the relaxation time of chiral density for one-pion exchange (the green diamonds) and σ exchange (the maroon squares) versus temperature. On the left panel we plot the results obtained by the Boltzmann kernel in Eq. (8); on the right panel we show our results obtained by the Fermi-Dirac kernel in Eq. (11). One of the most interesting aspects of data shown in Fig. 4 is the qualitative behavior of the relaxation time versus temperature: we find that regardless of the interaction channel chosen, as well as the statistics used in the collision integral, τ decreases with temperature. The lowering of τ is more evident in the low-temperature phase and in the crossover region, staying almost constant in the high-temperature phase.

In Fig. 4 we have shown the relaxation time for σ mesons and for pions. We find that the relaxation time of pions is always smaller than the one of σ mesons: in the low-temperature phase this is mainly due to the larger mass of the latter in comparison with that of pions, see Fig. 3. In the high-temperature phase, where $m_\sigma \simeq m_\pi$, the relaxation time due to σ exchange is still larger than the one obtained by pions: as a matter of fact, even if diagram (a) in Fig. 1 is equal to diagram (a) in Fig. 2, the multiplicity of diagrams for π-mediated scattering is larger than the one for σ exchange, implying that the former has a larger scattering rate and a smaller relaxation time.

It is interesting to compare the results obtained by using the Boltzmann kernel (8) in Eq. (26) with those obtained by the Fermi-Dirac kernel (11), shown in Fig. 4 on left and right panel, respectively. As expected, the use of the correct Fermi-Dirac statistics leads to a slight increase of the relaxation time, corresponding to a lowering of the collision rate. This is due to the Pauli blocking factors in the collision integral that effectively reduce the phase space available for the collisions.

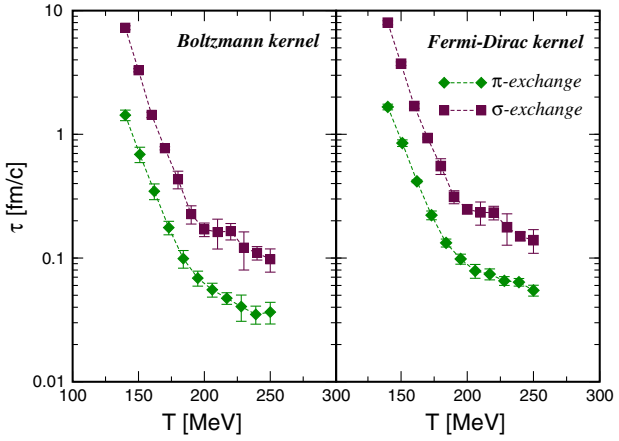

FIG. 4. Relaxation time of chiral density for one-pion exchange (green diamonds) and σ exchange (maroon squares) versus temperature. In the left panel we plot the results obtained by the Boltzmann kernel; on the right panel we show our results obtained by the Fermi-Dirac kernel.

The response of τ to temperature might sound counterintuitive, as one might expect that by increasing temperature chiral symmetry gets restored so the processes able to flip chirality of quarks, which are naively expected to be governed by M_q, should be suppressed and τ should increase. However, a closer analysis of the problem shows that it is not so trivial and one has to consider carefully all the factors governing the relaxation time, which are the phase space available for collisions on the one hand, and the interaction strength on the other hand. As a matter of fact, although the effective coupling strength among quarks and pions can decrease with temperature, the phase space available for collisions becomes larger thanks to smaller quark masses and larger temperature, which broadens the distribution functions.

This property can be illustrated by computing

$$J = |\mathcal{M}(t,u)|^2 \frac{\partial F(t,u)}{\partial \mu_5}\bigg|_{\mu_5=0}, \tag{61}$$

where (t,u) correspond to the Mandelstam variables and F corresponds to the kernel of the collision integral either in Eq. (8) or (11), whose derivative with respect to μ_5 at $\mu_5 = 0$ enters in the linearized collision rate (16). The quantity J can be interpreted as the squared matrix element weighted by distribution functions. We limit this discussion to the case of π-mediated scattering and to the Fermi-Dirac kernel in Eq. (8), since other cases do not differ qualitatively from this one. In Fig. 5 we plot J versus $\beta\sqrt{-t}$ and $\beta\sqrt{-u}$ with $\beta = 1/T$ for several values of temperatures, for the case of one-pion exchange and the Fermi-Dirac kernel in the collision integral. Plots on the right column are contour representations of the same quantities shown on the left column. From upper to lower panels we plot J for $T = 150$ MeV, which is below T_c, for $T = T_c$, and finally, for $T = 210$ MeV.

We notice that by increasing temperature the magnitude of weighted matrix element J becomes gradually smaller; hence the scattering matrix itself becomes less efficient in producing chirality changes in the thermal bath. On the other hand, J spreads in momentum space as temperature is increased: in fact from the data shown in the contour plots in the figure, results show that increasing temperature J gets its larger contribution from the square $0 \le \beta\sqrt{-t} \le 5$, $0 \le \beta\sqrt{-u} \le 5$ in momentum space, which covers a fraction of phase space growing as T^2 with temperature. As a consequence, the amount of phase space occupied by quarks and giving a contribution to the collision integral increases with temperature, competing against the lowering of the scattering matrix and eventually leading to the increase of the collision rate.

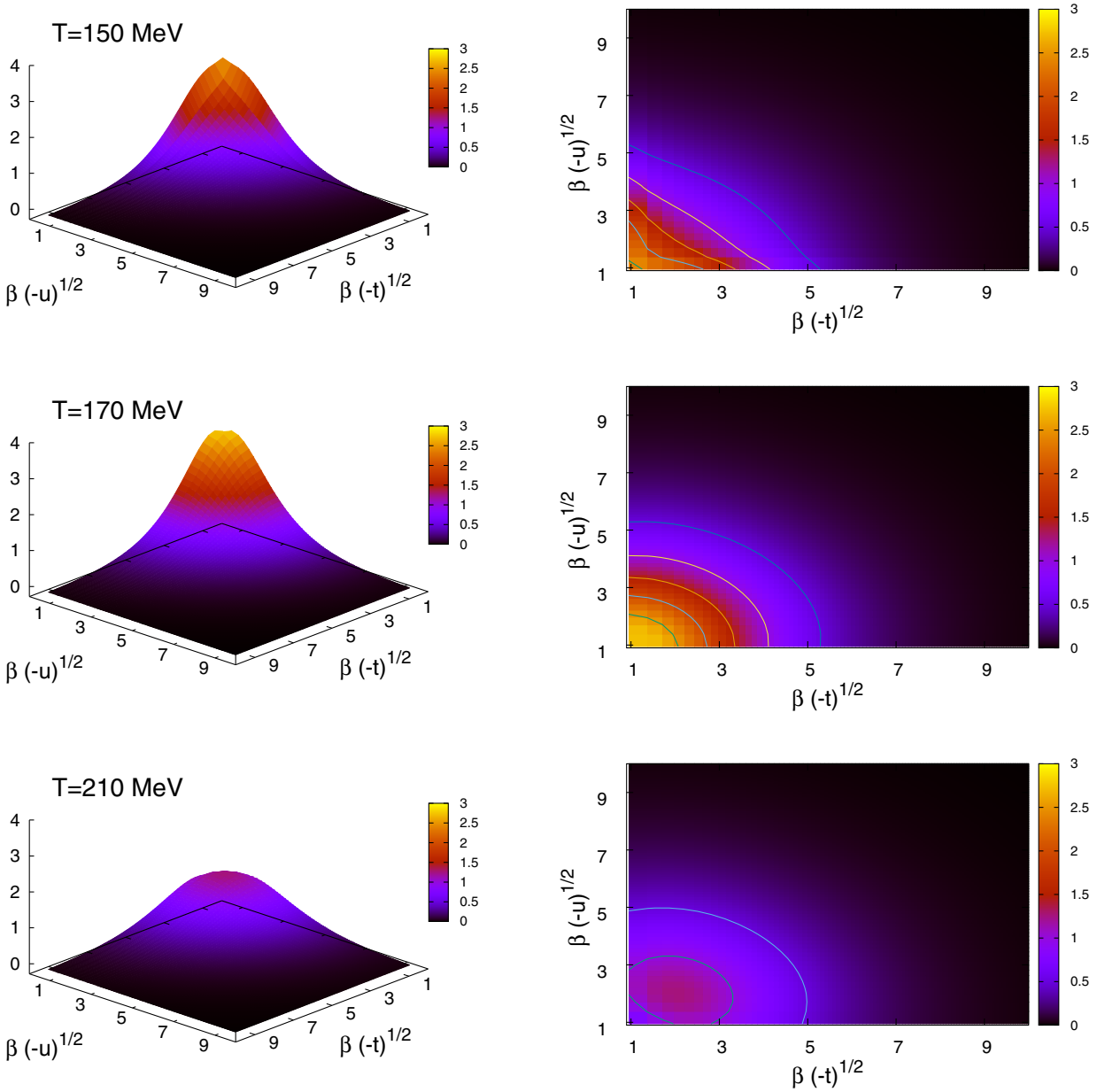

FIG. 5. The weighted matrix element J, Eq. (61), as a function of $\beta\sqrt{-t}$ and $\beta\sqrt{-u}$, with $\beta = 1/T$, for several values of temperatures, for the case of one-pion exchange and the Boltzmann kernel in the collision integral. The plots in the right column are contour representations of the corresponding quantities in the left column.

We can elaborate more on the role of the effective phase space opening with temperature by computing the collision rate with $|\mathcal{M}|^2 = 1$ in Eq. (6): in this way we remove every detail about collisions, and Γ reacts only to the variation of the distribution functions, hence measuring the amount of momentum space involved in the collisions. In Fig. 6 we plot Γ with $|\mathcal{M}|^2 = 1$ versus temperature for the cases of Boltzmann (red triangles) and Fermi-Dirac (green squares) statistics. In both cases we find a noticeable increase of this Γ in the crossover region: changing T from 150 to 200 MeV we find $\Gamma(T = 200)/\Gamma(T = 150) \simeq 18$ for the case of the Boltzmann kernel, and $\Gamma(T = 200)/\Gamma(T = 150) \simeq 11$ for the case of the Fermi-Dirac kernel.

B. Hybridization of the NJL model with a quasiparticle model

Although the NJL model offers a nice qualitative description of the chiral crossover at finite temperature, it is likely to miss the description of relevant degrees of freedom above T_c. As a matter of fact, quarks in the NJL model above T_c have in the chiral limit a vanishing mass within the mean field approximation; on the other hand it is known that at large temperatures quarks develop a chirally

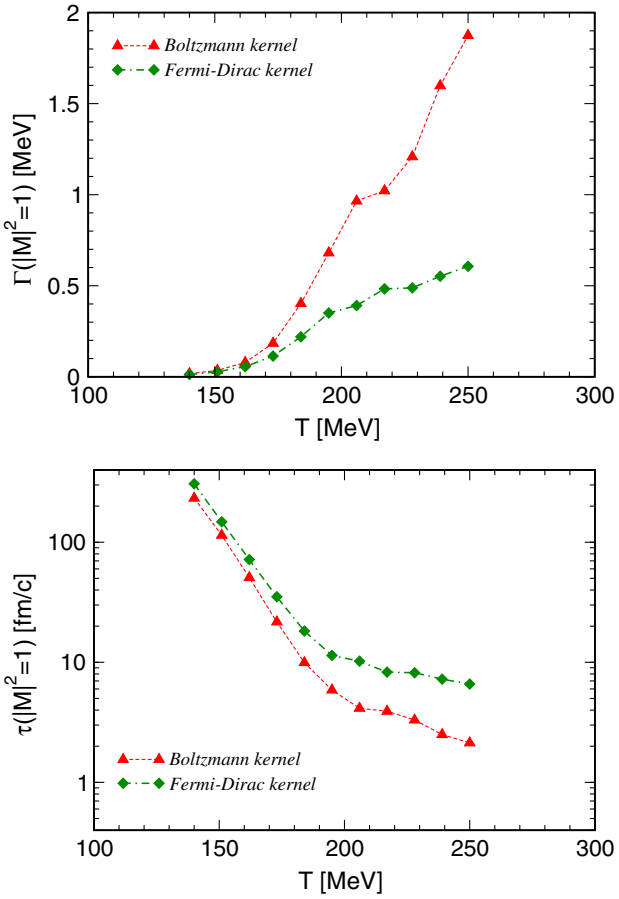

FIG. 6. Upper panel: Collision rate with $|\mathcal{M}|^2 = 1$ for Boltzmann (red triangles) and Fermi-Dirac (green squares) kernels. Lower panel: relaxation time with $|\mathcal{M}|^2 = 1$.

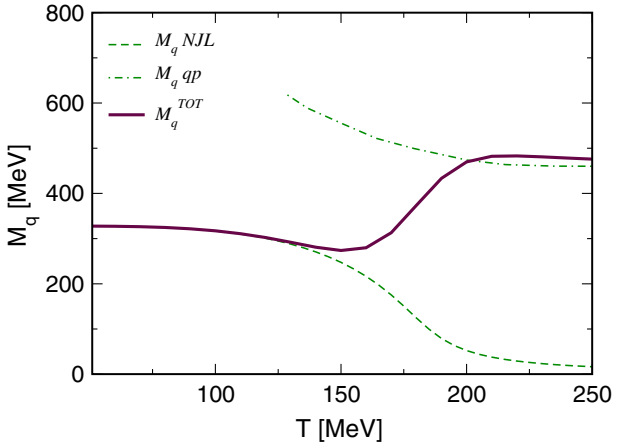

FIG. 7. Constituent quark mass computed by the NJL model (the dashed line), quasiparticle thermal mass (dot-dashed line), and interpolation among the two (the solid line) used in the calculation of the relaxation time.

invariant self-energy that generates a thermal pole mass, $M_T \propto gT$, due to the QCD interactions, and this thermal mass increases with temperature. Evading the chiral limit by adding a small current quark mass in the NJL model does not change the fact that M_q decreases with temperature and $M_q \ll T$ for $T > T_c$. There are, however, quasiparticle models inspired by the behavior of the thermal mass in QCD at $T \gg T_c$, in which one assumes that a quasiparticle description is valid also at temperatures $T \simeq T_c$; see for example [43–52]. In these models typically one assumes $M_T \propto gT$ with g corresponding to a temperature dependent strong coupling constant fixed by a numerical fit to lattice data from $T \simeq T_c$ up to very large temperatures.

In Fig. 7 we plot the constituent quark mass M_q computed by the NJL model (the dashed line), compared to the quasiparticle thermal mass M_T (the dot-dashed line) computed in Ref. [44]. The main difference between these two masses, M_q and M_T, is that the latter—contrary to the former—is not related to a term $\propto \bar{\psi}\psi$ in the quark Lagrangian, being rather related to many body effects at finite temperature that induce a pole in the full quark propagator. While this concept is rigorous at very large temperature, in quasiparticle models one assumes for simplicity that the pole mass is still a meaningful concept at the chiral crossover.

Assuming the point of view of a quasiparticle model implies that above T_c quark mass can be quite large even if chiral symmetry is restored: this can affect the collision rate because of the reduction of momentum space occupied by quarks. We find it therefore interesting to compute the relaxation time of chiral density assuming a quasiparticle nature of quarks above T_c. We achieve this by using a model for the quark mass that interpolates between the low-temperature NJL quark mass $M = M_q(T)$ and the high-temperature thermal quark mass $M_T = M_T(T)$, shown by the solid orange line in Fig. 7. The interpolating function we use is

$$M(T) = M_q(T) + a(T)M_T(T), \tag{62}$$

where the function $a(T)$ is given by

$$a(T) = \frac{1}{2}\left[1 + \tanh\left(\frac{T - T_0}{c}\right)\right]. \tag{63}$$

In the above equation M_q corresponds to the solution of the NJL gap equation, and M_T is the quasiparticle mass obtained by the fit of the corresponding lattice data in [44]. The two numerical parameters are chosen as $T_0 = 180$ MeV and $c = 20$ MeV. The functional form in Eq. (62) is not the solution of a gap equation: it is chosen only to interpolate smoothly between M_q and M_T in the crossover region, with the purpose of illustrating the effect of turning from the NJL model to the quasiparticle one on the relaxation time.

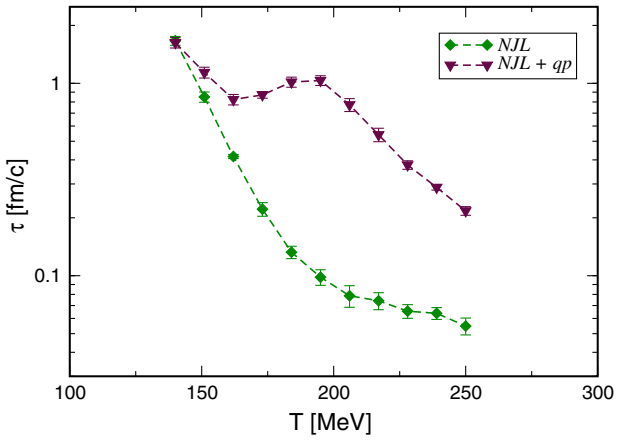

FIG. 8. The chiral relaxation time for the NJL model (the green diamonds) and NJL + qp model (the maroon triangles).

In Fig. 8 we plot the relaxation time versus temperature for the cases of the pure NJL model (green diamonds) and NJL model hybridized with a quasiparticle model (maroon triangles); in both cases we have used the Fermi-Dirac kernel in the collision integral. We find that the overall effect of the quasiparticle model mass is to increase the relaxation time: as a matter of fact the increase of quark mass induces a lowering of the available phase space for the collisions, leading to a smaller collision rate and a larger relaxation time in comparison with the NJL calculation. Although relaxation time within the quasiparticle model is larger than the one we obtain within the NJL model, the effect of increasing temperature leads to a nonmonotonic behavior of the relaxation rate τ: in fact the increasing of M given by Eq. (62) has to compete with the increase of temperature that opens phase space and increases the collision rate.

V. CONCLUSIONS

In this article we have studied relaxation of chiral density, n_5, in the two flavor NJL model that describes in simple terms the chiral crossover of QCD at a temperature $T_c \simeq 170$ MeV. In particular, we have computed the relaxation time for chiral density τ (the chiral relaxation time), which is associated with the scattering of quarks via one-pion and one-σ-meson exchanges. These processes are good candidates for inducing chirality flips in quark matter around the chiral crossover within the effective-model approach based on the NJL model.

In order to compute the chiral relaxation time, τ, we have followed the well-established formalism to deal with quark scattering within the NJL model. First, we evaluated the finite-temperature π- and σ-meson propagators within the random phase approximation. Secondly, we calculated scattering amplitudes due to meson exchanges. Thirdly, we used the latter to compute the collision integral for the chirality-changing processes that is directly related to the relaxation of the chiral density, dn_5/dt, and we used again the NJL model to relate the chiral density n_5 with chiral chemical potential μ_5 in the thermal bath. We assumed a weak chiral imbalance $\mu_5 \ll T$ in order to be able to work at the lowest order in μ_5/T that allowed us to drastically simplify the computation of the collision integral. Finally, we compute the collision rate Γ and the chiral relaxation time τ via the relation $\Gamma = -(dn_5/dt)/n_5$. We focused on a temperature range around the chiral crossover because at this region the quark degrees of freedom should have solid physical meaning.

We found that the results for the chiral relaxation time τ do not depend on the statistics used to calculate the collision integral as, according to Fig. 4, both Boltzmann and Fermi-Dirac distributions give very similar results in the chiral crossover region. Moreover, the same figure demonstrates that the chiral relaxation time τ_σ due to the σ-meson exchange is much larger compared to the relaxation time τ_π corresponding to the pion exchanges, $\tau_\sigma \gg \tau_\pi$. This feature can be explained by the fact that in the low-temperature phase the σ exchange is suppressed because σ-meson mass is larger than pion mass. Around and above the chiral crossover the masses are of the same order, $m_\sigma \simeq m_\pi$, but still the relaxation time related to the σ exchange is much larger compared to the one of the pion exchange due to larger number of the diagrams that contribute to the latter. Thus, the pion exchanges are dominating the chiral relaxation processes.

We have computed also the relaxation time in the hybridized NJL model, where the constituent quark's mass in the chirally restored region is tuned to the thermal mass of the quarks obtained by a fit to lattice data about QCD thermodynamics in [44]. Our results for the chiral relaxation time τ in the chiral crossover region are summarized in Fig. 8. We find that regardless of the choice of the thermal quark mass, the chiral relaxation time follows an almost monotonic behavior with increasing temperature, even if the effect of the thermal mass is to keep τ higher compared to the one computed within the NJL model. Globally, the relaxation time falls down with the increase of the temperature from $\tau \simeq 1$ fm at the lower-temperature end of the crossover at $T \simeq 150$ MeV till much faster chiral flips, $\tau \simeq 0.1$ fm at higher temperature at $T \simeq 250$ MeV. The fast increase of the collision rate (i.e., the lowering of τ) with rising temperature can be understood as a combination of two factors: on the one hand, the scattering matrix weighted by the distribution functions decreases with temperature, but on the other hand it also broadens in the momentum space, thus effectively leading to a growing of the phase space volume involved in collisions. The latter dominates over the former, thus enhancing the collision rate and lowering the relaxation time with increase of temperature.

ACKNOWLEDGMENTS

M. R. and G. X. P. thank the CAS President's International Fellowship Initiative (Grant No. 2015PM008), and the NSFC projects (Grants No. 11135011 and No. 11575190). M. R. acknowledges discussions with F. Scardina. The source code for the implementation of pseudorandom and low discrepancy sequences used in our numerical calculations is distributed under the GNU-LGPL license and can be found on the John Burkardt Fortran 90 Source Codes website.

[1] S. L. Adler, Phys. Rev. **177**, 2426 (1969).
[2] J. S. Bell and R. Jackiw, Nuovo Cimento A **60**, 47 (1969).
[3] G. D. Moore, arXiv:hep-ph/0009161.
[4] G. D. Moore and M. Tassler, J. High Energy Phys. 02 (2011) 105.
[5] D. E. Kharzeev, L. D. McLerran, and H. J. Warringa, Nucl. Phys. **A803**, 227 (2008).
[6] K. Fukushima, D. E. Kharzeev, and H. J. Warringa, Phys. Rev. D **78**, 074033 (2008).
[7] Q. Li, D. E. Kharzeev, C. Zhang, Y. Huang, I. Pletikosić, A. V. Fedorov, R. D. Zhong, J. A. Schneeloch, G. D. Gu, and T. Valla, Nat. Phys. **12**, 550 (2016).
[8] D. T. Son and P. Surowka, Phys. Rev. Lett. **103**, 191601 (2009).
[9] N. Banerjee, J. Bhattacharya, S. Bhattacharyya, S. Dutta, R. Loganayagam, and P. Surowka, J. High Energy Phys. 01 (2011) 094.
[10] K. Landsteiner, E. Megias, and F. Pena-Benitez, Phys. Rev. Lett. **107**, 021601 (2011).
[11] D. T. Son and A. R. Zhitnitsky, Phys. Rev. D **70**, 074018 (2004).
[12] M. A. Metlitski and A. R. Zhitnitsky, Phys. Rev. D **72**, 045011 (2005).
[13] D. E. Kharzeev and H. U. Yee, Phys. Rev. D **83**, 085007 (2011).
[14] M. N. Chernodub, J. High Energy Phys. 01 (2016) 100.
[15] M. N. Chernodub and M. Zubkov, arXiv:1508.03114.
[16] M. N. Chernodub, A. Cortijo, A. G. Grushin, K. Landsteiner, and M. A. H. Vozmediano, Phys. Rev. B **89**, 081407 (2014).
[17] V. Braguta, M. N. Chernodub, K. Landsteiner, M. I. Polikarpov, and M. V. Ulybyshev, Phys. Rev. D **88**, 071501 (2013).
[18] A. V. Sadofyev and M. V. Isachenkov, Phys. Lett. B **697**, 404 (2011).
[19] A. V. Sadofyev, V. I. Shevchenko, and V. I. Zakharov, Phys. Rev. D **83**, 105025 (2011).
[20] Z. V. Khaidukov, V. P. Kirilin, A. V. Sadofyev, and V. I. Zakharov, arXiv:1307.0138.
[21] V. P. Kirilin, A. V. Sadofyev, and V. I. Zakharov, arXiv:1312.0895.
[22] A. Avdoshkin, V. P. Kirilin, A. V. Sadofyev, and V. I. Zakharov, Phys. Lett. B **755**, 1 (2016).
[23] M. Ruggieri and G. X. Peng, Phys. Rev. D **93**, 094021 (2016).
[24] M. Ruggieri and G. X. Peng, arXiv:1602.03651.
[25] M. Ruggieri and G. X. Peng, arXiv:1602.05250 [J. Phys. G (to be published)].
[26] R. Gatto and M. Ruggieri, Phys. Rev. D **85**, 054013 (2012).
[27] K. Fukushima, M. Ruggieri, and R. Gatto, Phys. Rev. D **81**, 114031 (2010).
[28] M. N. Chernodub and A. S. Nedelin, Phys. Rev. D **83**, 105008 (2011).
[29] M. Ruggieri, Phys. Rev. D **84**, 014011 (2011).
[30] L. Yu, H. Liu, and M. Huang, Phys. Rev. D **94**, 014026 (2016).
[31] L. Yu, J. Van Doorsselaere, and M. Huang, Phys. Rev. D **91**, 074011 (2015).
[32] M. Frasca, arXiv:1602.04654.
[33] V. V. Braguta, E.-M. Ilgenfritz, A. Y. Kotov, B. Petersson, and S. A. Skinderev, Phys. Rev. D **93**, 034509 (2016).
[34] V. V. Braguta, V. A. Goy, E.-M. Ilgenfritz, A. Y. Kotov, A. V. Molochkov, M. Muller-Preussker, and B. Petersson, J. High Energy Phys. 06 (2015) 094.
[35] V. V. Braguta and A. Y. Kotov, Phys. Rev. D **93**, 105025 (2016).
[36] M. Hanada and N. Yamamoto, *Proc. Sci.*, LATTICE2011 (2011) 221 [arXiv:1111.3391].
[37] S. S. Xu, Z. F. Cui, B. Wang, Y. M. Shi, Y. C. Yang, and H. S. Zong, Phys. Rev. D **91**, 056003 (2015).
[38] B. Wang, Y. L. Wang, Z. F. Cui, and H. S. Zong, Phys. Rev. D **91**, 034017 (2015).
[39] D. Ebert, T. G. Khunjua, K. G. Klimenko, and V. C. Zhukovsky, Phys. Rev. D **93**, 105022 (2016).
[40] S. S. Afonin, A. A. Andrianov, and D. Espriu, Phys. Lett. B **745**, 52 (2015).
[41] A. A. Andrianov, D. Espriu, and X. Planells, Eur. Phys. J. C **73**, 2294 (2013).
[42] R. L. S. Farias, D. C. Duarte, G. Krein, and R. O. Ramos, arXiv:1604.04518.
[43] M. I. Gorenstein and S. N. Yang, Phys. Rev. D **52**, 5206 (1995).
[44] S. Plumari, W. M. Alberico, V. Greco, and C. Ratti, Phys. Rev. D **84**, 094004 (2011).
[45] P. Levai and U. W. Heinz, Phys. Rev. C **57**, 1879 (1998).
[46] M. Bluhm, B. Kampfer, and G. Soff, Phys. Lett. B **620**, 131 (2005).
[47] M. Bluhm, B. Kampfer, R. Schulze, D. Seipt, and U. Heinz, Phys. Rev. C **76**, 034901 (2007).
[48] P. Castorina, D. E. Miller, and H. Satz, Eur. Phys. J. C **71**, 1673 (2011).
[49] P. Alba, W. Alberico, M. Bluhm, V. Greco, C. Ratti, and M. Ruggieri, Nucl. Phys. **A934**, 41 (2015).
[50] M. Ruggieri, P. Alba, P. Castorina, S. Plumari, C. Ratti, and V. Greco, Phys. Rev. D **86**, 054007 (2012).
[51] L. Oliva, P. Castorina, V. Greco, and M. Ruggieri, Phys. Rev. D **88**, 097502 (2013).

[52] V. Begun, W. Florkowski, and R. Ryblewski, arXiv: 1602.08308.
[53] H. J. Warringa, Phys. Rev. D **86**, 085029 (2012).
[54] A. Y. Babansky, E. V. Gorbar, and G. V. Shchepanyuk, Phys. Lett. B **419**, 272 (1998).
[55] G. Cao and X. G. Huang, Phys. Lett. B **757**, 1 (2016).
[56] C. Manuel and J. M. Torres-Rincon, Phys. Rev. D **92**, 074018 (2015).
[57] Y. Nambu and G. Jona-Lasinio, Phys. Rev. **122**, 345 (1961).
[58] Y. Nambu and G. Jona-Lasinio, Phys. Rev. **124**, 246 (1961).
[59] S. P. Klevansky, Rev. Mod. Phys. **64**, 649 (1992).
[60] T. Hatsuda and T. Kunihiro, Phys. Rep. **247**, 221 (1994).
[61] R. E. Caflisch, Acta Numer. **7**, 1 (1998).
[62] H. Niederreiter, Bull. Am. Math. Soc. **84**, 6 (1978).
[63] W. H. Press and G. R. Farrar, Comput. Phys. **4**, 190 (1990).
[64] W. H. Press *et al.*, *Numerical Recipes: The Art of Scientific Computing* (Cambridge University Press, Cambridge, 2007).
[65] I. M. Sobol, USSR Computational Mathematics and Mathematical Physics **16**, 236 (1976).